

# Magnetic evidence for hot superconductivity in multi-walled carbon nanotubes

Guo-meng Zhao\* and Pieder Beeli

*Department of Physics and Astronomy, California State University, Los Angeles, CA 90032, USA*

We report magnetic measurements up to 1200 K on three different multi-walled carbon nanotube mat samples using Quantum Design vibrating sample magnetometers with an ultra low-field option. Three different samples prepared from arc discharge or chemical vapor deposition contain magnetic impurities ranging from about 100 ppm to about 1.5%. Our extensive magnetic data consistently show two superconducting transitions, one at temperatures between 550 K and 720 K, and another at about 1200 K. The first transition temperature  $T_{cJ}$ , which coincides with the transition temperature seen in the resistance data, depends very strongly on the magnetic field, as expected from the onset of intergrain Josephson coupling. The strong field dependence of  $T_{cJ}$  also excludes magnetic contaminants as the origin of the first transition. A large paramagnetic susceptibility (12% of  $1/4\pi$ ) is observed at 1140 K for the most pure sample in a field of 0.03 Oe and this susceptibility decreases rapidly with increasing field. On the other hand, the most impure sample shows a large diamagnetic susceptibility (3% of  $-1/4\pi$ ) at 1000 K. These data can *only* be explained by a scenario where paramagnetic susceptibility—due to circulating currents around vortices (paramagnetic Meissner effect)—competes with diamagnetic susceptibility—due to diamagnetic shielding currents. The present results provide compelling evidence for superconductivity well above room temperature in multi-walled carbon nanotubes.

## I. INTRODUCTION

It is generally believed that the superconducting transition temperature  $T_c$  cannot be higher than 30 K within the conventional phonon-mediated mechanism although there is no theoretical justification for this  $T_c$  limit. Alexandrov and Mott have demonstrated that the Bose-Einstein condensation of bipolarons can explain high-temperature superconductivity in cuprates [1]. Ginzburg [2] and Little [3] have proposed that high-temperature superconductivity could be realized by exchanging high-energy electronic excitations such as excitons and plasmons. Lee and Mendoza have shown that superconductivity as high as 500 K can be reached through a pairing interaction mediated by undamped acoustic plasmon modes in a quasi-one-dimensional (1D) electronic system [4]. Moreover, high-temperature superconductivity can occur in a multi-layer electronic system due to an attraction of charge carriers in the same conducting layer via exchange of virtual plasmons in neighboring layers [5]. If these plasmon-mediated pairing mechanisms are relevant, one should be able to find high-temperature superconductivity in quasi-one-dimensional and/or multi-layer systems such as cuprates, carbon nanotubes (CNTs), and graphites.

Carbon nanotubes constitute a novel class of quasi-one-dimensional materials which offer the potential for high-temperature superconductivity. The simplest single-walled nanotube (SWNT) consists of a single graphite sheet which is curved into a long cylinder, with a diameter which can be smaller than 1 nm. Band-structure calculations predict that carbon nanotubes have two types of electronic structures depending on the chirality [6,7], which is indexed by a chiral vector  $(n, m)$ :  $n - m = 3N + \nu$ , where  $N, n, m$  are the integers, and  $\nu =$

$0, \pm 1$ . The tubes with  $\nu = 0$  are metallic while the tubes with  $\nu = \pm 1$  are semiconductive. For metallic chirality SWNTs, there are two and six transverse conduction channels when the Fermi level is crossing the first and second subbands, respectively. Multiwalled nanotubes (MWNTs) consist of at least two concentric shells which can have different chiralities. The outer diameters of our arc discharge prepared MWNTs are centered around 10-15 nm. The MWNTs possess both quasi-one-dimensional and multi-layer electronic structures. This unique quasi-one-dimensional electronic structure in both SWNTs and MWNTs make them ideal for plasmon-mediated high-temperature superconductivity.

In order to confirm the existence of superconductivity, it is essential to provide two important signatures: the Meissner effect and the resistive transition. In 2001 Zhao *et al.* [8] provided magnetic and electrical evidence for possible superconductivity above room temperature in MWNT mat samples. The resistivity data show a possible superconductive transition at about 700 K. Due to the granular nature of the mat samples, intertube barrier resistance below 700 K does not go to zero and the temperature dependence of the barrier resistance is proportional to  $\exp(-bT)$ , as expected for the insulating granular superconductivity [9]. Since then, Zhao [10-17] has analyzed previously published magnetic, electrical, and optical data for both single-walled and multi-walled carbon nanotubes, and provided over twenty pieces of evidence for the existence of superconductivity above room temperature. In 2003, Kopelevich and coworkers [18] gave magnetic evidence for local superconductivity up to 270 K in graphite-sulfur composites. The observations of hot superconductivity in carbon nanotubes and graphite-sulfur composites suggest a common microscopic origin of superconductivity.

In this article, we report magnetic measurements up to 1200 K on three different multi-walled carbon nanotube mat samples using sensitive vibrating sample magnetometers (VSMs) from Quantum Design. The ultra-low-field option of the VSM system allows us to do the magnetization measurements in a field as low as 0.03 Oe. One sample is prepared from arc discharge (denoted as ARC) and contains about 46 ppm  $\text{Fe}_3\text{O}_4$ . The second sample is prepared from chemical vapor deposition (denoted as CVD1) and contains about 1.5%  $\text{Fe}_3\text{O}_4$ . The third sample is also prepared from chemical vapor deposition (denoted as CVD2) and has about 0.3%  $\text{Fe}_2\text{O}_3$ . Our extensive magnetic data consistently show two superconducting transitions, one at about 703 K, 550 K, and 720 K for sample ARC, sample CVD1 and sample CVD2, respectively, and another at about 1200 K. The first transition temperature  $T_{cJ}$ , which coincides with the transition temperature seen in the resistance data, depends very strongly on the magnetic field, as expected from the onset of intergrain Josephson coupling. The strong field dependence of  $T_{cJ}$  also excludes magnetic contaminants as the origin of the first transition. Above 1000 K, no magnetic remanences are seen, which excludes magnetic impurities with Curie-temperatures higher than 1000 K. The superconducting remanent magnetization, which can be separated from the contribution of magnetic impurities, disappears above  $T_{cJ}$  for each of the three samples. The large paramagnetic susceptibility (12% of  $1/4\pi$ ) is observed at 1140 K for the most pure sample in a field of 0.03 Oe and this susceptibility decreases rapidly with increasing field. On the other hand, the most impure sample shows a large diamagnetic susceptibility (3% of  $-1/4\pi$ ) at 1000 K. These data can *only* be explained by a scenario [19] where paramagnetic susceptibility—due to circulating currents around vortices (paramagnetic Meissner effect)—competes with diamagnetic susceptibility—due to diamagnetic shielding currents. The present results provide compelling evidence for superconductivity well above room temperature in multi-walled carbon nanotubes.

## II. EXPERIMENT

### A. Sample characterization

Three different multi-walled carbon nanotube mat samples are obtained from the SES Research of Houston. Sample ARC is prepared from an arc discharge process with no metal catalysts. The nanotubes consist of 5-20 graphite layers with 2-20 nm in diameter and 100 nm to 2  $\mu\text{m}$  in length. The tubes are normally assembled into bundles, and the bundles are assembled into mats. Sample ARC comes from the same lot as those studied in Ref. [8]. This sample contains a total of about 100 ppm magnetic impurities, as determined from the magnetic measurement (see below). The mass of sample ARC—for

most magnetic measurements—is 41 mg. Sample CVD1 is prepared from chemical vapor deposition and the sample contains about 1.5%  $\text{Fe}_3\text{O}_4$ . The mass of sample CVD1 is 5 mg. Sample CVD2 is also prepared from chemical vapor deposition and contains a total of about 0.3% impurities as specified by the SES Research. The mass of sample CVD2 is 11 mg.

### B. Measurements

Magnetization was measured by two Quantum Design vibrating sample magnetometers (VSMs). We attain high accuracy in the measurements with 10 second per point averaging (the precision is better than  $2 \times 10^{-7}$  emu). A field between 0.03 Oe and 15 Oe can be achieved using the ultra low-field option. The magnitude and direction of the field profile were measured by the flux-gate device. For the oven option, the temperature limit is rated up to 1000 K, but we successfully pushed the temperature up to 1200 K in three runs on sample ARC. In the fourth run, the oven heater broke at about 1132 K. The sample chamber is in a high vacuum ( $<10^{-4}$  torr) during measurements, which prevents the carbon nanotubes from burning. The VSM oscillation frequency is 40 Hz and the oscillation amplitude is 1 mm. When the sample is inserted into the sample chamber, the sample first experiences about 200 Oe positive (upward) field and then the same negative field (downward) due to the presence of the linear motor for vibrating the sample. The magnetic hysteresis loop was measured for the sample holder (including the heater sticker, Zircar cement, and copper foil) at 300 K. The saturation moment is  $5.4 \times 10^{-6}$  emu and the linear moment per Oe is  $-4.3 \times 10^{-9}$  emu. Such a saturation moment corresponds to about  $5.4 \times 10^{-5}$  mg of magnetic impurities if we take a typical saturation magnetization of 100 emu/g. Our sample masses range from 5 mg to 41 mg, which are  $10^5$ - $10^6$  times larger than the mass of magnetic impurities in the sample holder. Therefore, the magnetic signal from the sample holder is negligible compared with our sample signals.

## III. RESULTS AND DISCUSSIONS

### A. Superconductivity in sample CVD2

Fig. 1a shows the temperature dependence of the magnetization in a field of 0.03 Oe for sample CVD2. When the sample was inserted into the sample chamber at 300 K, the sample was first exposed to about 200 Oe positive (upward) field and then to the same negative (downward) field due to the presence of the linear motor for vibrating the sample. One can see that the magnetization is negative below 902 K, which would be mistakenly taken as evidence of superconductivity at 902 K if so interpreted.

In fact, the negative magnetization is the sum of the remanences of ferromagnetic impurities and/or superconductors because the sample has experienced about  $-200$  Oe field before being subject to the  $0.03$  Oe field. The remanence should disappear at a temperature above which the warm-up magnetization coincides with the cool-down magnetization. Fig. 1b shows an expanded view of the magnetization in the positive magnetization region. One can clearly see that above  $960$  K the warm-up data coincide with the cool-down data within the experimental uncertainty, suggesting a ferromagnetic/ferrimagnetic transition at about  $960$  K. The data also imply that there are no ferromagnetic/ferrimagnetic impurities with Curie temperatures higher than  $960$  K and coercivities higher than  $0.03$  Oe.

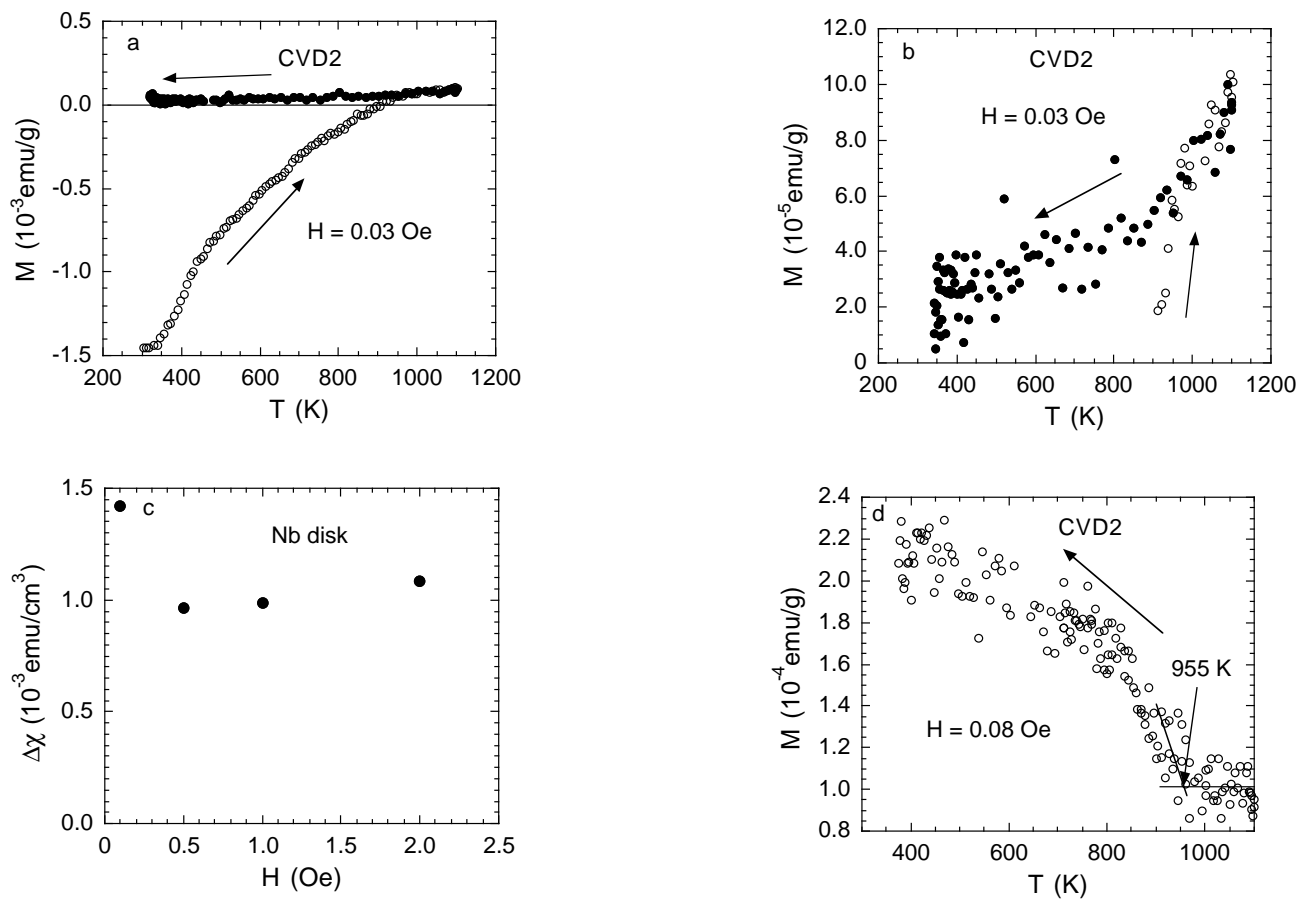
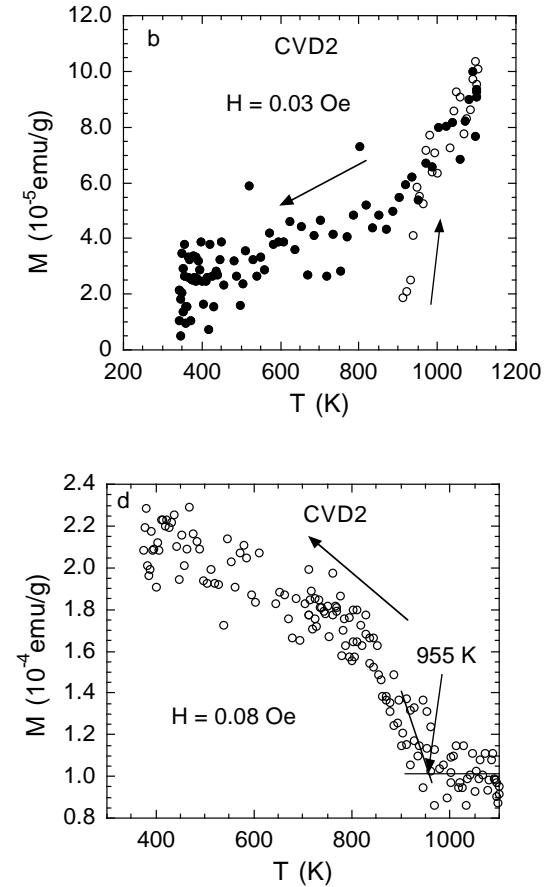


FIG. 1. a) The temperature dependence of the magnetization in a field of  $0.03$  Oe for sample CVD2. b) The expanded view of the magnetization in the positive magnetization region in the field of  $0.03$  Oe for sample CVD2. c) The difference between the peak susceptibility near  $T_c$  and the susceptibility at  $0.93T_c$  for a Nb disk. The data are extracted from Fig. 1 of Ref. [20]. d) The temperature dependence of the magnetization in a field of  $0.08$  Oe for sample CVD2. The susceptibility at  $1100$  K is  $3.4 \times 10^{-3}$  emu/g in the field of  $0.03$  Oe and  $1.26 \times 10^{-3}$  emu/g in the field of  $0.08$  Oe. The ferrimagnetic component of the susceptibility at  $700$  K is  $9.9 \times 10^{-4}$  emu/g (the difference of the susceptibilities at  $700$  K and  $1000$  K).

It is interesting that the cool-down magnetization decreases sharply with decreasing temperature in the temperature region between  $860$  K and  $1100$  K. The temperature dependence for this sample is similar to the para-

magnetic Meissner effect (PME) observed in a Nb disk (see Fig. 1 of [20]). Such a temperature dependence can arise from the interplay between the diamagnetic screening currents (diamagnetic Meissner effect) and the paramagnetic circulating currents around the vortices [19]. The diamagnetic component of the susceptibility should be nearly independent of the magnetic field  $H$  when  $H$  is below the lower critical field  $H_{c1}$ . This is indeed the case for the Nb disk, as shown in Fig. 1c where we plot the difference between the peak susceptibility near  $T_c$  and the susceptibility at  $0.93T_c$ . We see that the diamagnetic component is nearly independent of the field. On the other hand, for a granular superconductor, the lower critical field tends to zero due to a very large intergrain penetration depth. In the low field region, the magnitude of the diamagnetic susceptibility is found to increase



much faster than  $1/H$  (see Ref. [21–23]) while the paramagnetic Meissner susceptibility is nearly independent of the field (see Fig. 5c and Fig. 8 below). Thus the diamagnetic component can be comparable with the para-

magnetic Meissner susceptibility in the low field range. In the high field region, the paramagnetic Meissner susceptibility decreases faster than  $1/H$  (see Fig. 5c below) while the diamagnetic component has a weak field dependence (see Fig. 7 of Ref. [21]). In this case, it is possible that the diamagnetic Meissner effect can overwhelm the competing paramagnetic Meissner effect. In the intermediate field region, the paramagnetic Meissner effect will dominate.

Moshchalkov, Qiu, and Bruyndoncx (MQB) [19] suggested that the PME can be caused by the persistence of the giant vortex state with the fixed orbital quantum number  $L > 0$ . This state is formed in any finite-size superconductor at the third surface critical field  $H_{c3}$ , which is higher than the bulk upper critical field  $H_{c2}$  for smooth and clean surfaces. Clean multi-walled carbon nanotube superconductors are the ideal candidates for this theoretical model because of small diameters and cylindrical geometry. On the other hand, the PME will be greatly reduced if magnetic impurities suppress surface superconductivity substantially.

Another unusual feature in the cool-down data in 0.03 Oe is that there appears to be no signature of ferromagnetic ordering around 960 K. This can happen if the increasing rate of the ferromagnetic/ferrimagnetic susceptibility just below the Curie temperature is significantly lower than the decreasing rate of the intrinsic susceptibility of the carbon nanotubes. If the ferromagnetic/ferrimagnetic component of the susceptibility is independent of the field in the low field region, as it should be, and the intrinsic susceptibility of the carbon nanotubes and its temperature dependence decrease rapidly with the field, one should see the signature of this ferromagnetic/ferrimagnetic ordering in higher field magnetization data. Fig. 1d shows the field-cooled magnetization in a field of 0.08 Oe. In contrast to Fig. 1b, the data in Fig. 1d clearly show a ferromagnetic/ferrimagnetic ordering at about 955 K, confirming that the intrinsic susceptibility of the carbon nanotubes and its temperature dependence decrease rapidly with the field.

Indeed, the magnetization in 0.08 Oe is nearly independent of the temperature in the temperature region between 1000 K and 1100 K. In addition, the magnetization at 1100 K does not change with magnetic field within the experimental uncertainty. This field dependence of the magnetization in such a low field region is not expected for *any* kind of magnetic impurity, but is consistent with the paramagnetic Meissner effect. For  $\text{YBa}_2\text{Cu}_3\text{O}_{7-y}$  films, it is indeed found that the paramagnetic Meissner magnetization near the superconducting transition temperature is also independent of the field for fields less than 100 Oe (see Fig. 4 of [24]). This implies that the paramagnetic Meissner susceptibility near  $T_c$  is inversely proportional to the field  $H$ , that is, the paramagnetic Meissner magnetization can be saturated in very low fields.

If we consider the ferromagnetic/ferrimagnetic compo-

ment of the susceptibility, we may infer that the intrinsic susceptibility of the carbon nanotubes in 0.03 Oe is positive at 700 K but becomes negative at 350 K. The magnitude of the diamagnetic susceptibility at 350 K is estimated to be about  $6.3 \times 10^{-4}$  emu/g for sample CVD2 assuming that the paramagnetic susceptibility of the nanotubes in the field of 0.08 Oe is also independent of temperature below the Curie temperature. For sample CVD1 containing 1.5% magnetic impurities, the susceptibility in  $-0.06$  Oe is found to be  $-1.13 \times 10^{-3}$  emu/g at 1000 K (see Fig. 5 below). These results indicate that the sample with more magnetic impurities has a even larger diamagnetic component. Using the theoretical calculation for the orbital diamagnetism in carbon nanotubes [25], we estimate that the orbital diamagnetic susceptibility is about  $3 \times 10^{-6}$  emu/g at 350 K for nanotube shells with an average diameter of 8 nm and with a Fermi energy of 0.06 eV. The estimated magnitudes of the diamagnetic susceptibility in these mat samples exceed the orbital diamagnetic component by *at least two orders of magnitude*.

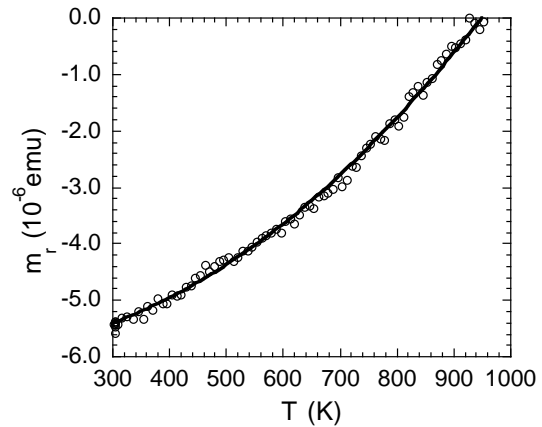


FIG. 2. The temperature dependence of the remanent moment for magnetic impurities in the  $\text{Er}_2\text{O}_3$  sample (about 8.6 mg) after the field was changed from about  $-200$  Oe to 0.08 Oe at 300 K. A small constant paramagnetic contribution from  $\text{Er}_2\text{O}_3$  has been subtracted from the data. The data can be well fitted by Eq. 1 with  $p = 2.07$ . These raw data also serve as a check on measurement accuracy.

The Curie temperature of 955 K suggests that the sample should contain  $\gamma\text{-Fe}_2\text{O}_3$  magnetic impurities. This is in agreement with our electron back-scattering data. Since we have identified  $\text{Fe}_2\text{O}_3$  as the major magnetic impurity, an independent measurement of the temperature dependence of the remanent magnetization for  $\gamma\text{-Fe}_2\text{O}_3$  under the same measurement conditions can provide important insight into the origin of the measured remanence in sample CVD2. It is fortunate that the magnetic measurement on an  $\text{Er}_2\text{O}_3$  sample (about 8.6 mg) in a field of 0.08 Oe also shows the existence of the magnetic remanence below about 950 K, as shown in Fig. 2. The para-

magnetic contribution from  $\text{Er}_2\text{O}_3$  has been subtracted from the data. The Curie temperature of 950 K suggests that the  $\text{Er}_2\text{O}_3$  sample also includes  $\gamma\text{-Fe}_2\text{O}_3$  impurities. We can fit the data in Fig. 2 by an equation

$$m_r(T) = m_r(0)[1 - (T/T_C)^p], \quad (1)$$

where  $m_r$  is the remanent moment. The best fit gives  $p = 2.07$ , which is very close to 2.

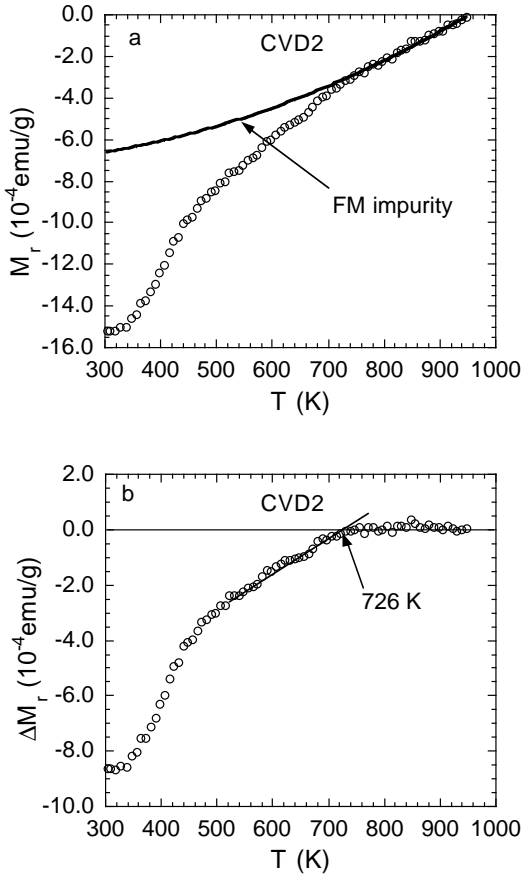


FIG. 3. a) The temperature dependence of the remanent magnetization for sample CVD2. b) The temperature dependence of the net remanent magnetization for the second component. The second component has a magnetic or a superconducting transition temperature of about 726 K.

In Fig. 3a, we show the remanent magnetization for sample CVD2. The small paramagnetic contribution due to the 0.03 Oe field has been subtracted. Comparing Fig. 3a with Fig. 2, we can clearly see that the temperature dependence of the remanent magnetization for sample CVD2 is very different from that for  $\gamma\text{-Fe}_2\text{O}_3$  magnetic impurities. By inspecting the data, we see that the remanent magnetization in Fig. 3a can be separated into two components, one for  $\gamma\text{-Fe}_2\text{O}_3$  magnetic impurities and second for the other magnetic impurities or for the superconducting nanotubes. Indeed, the data above 750 K can be well fitted by an

equation  $M_r(T) = M_r(0)[1 - (T/T_C)^{2.07}]$  (see the solid line). Fig. 3b shows the net remanent magnetization for the second component. It is apparent that the second component has a transition temperature of about 726 K. *A priori*, this transition could be *either* ferromagnetic/ferrimagnetic *or* superconducting. If it were a ferromagnetic/ferrimagnetic, the transition temperature *would* be independent of the magnetic field, and the field-cooled (FC) susceptibility *would* increase below the transition temperature and eventually saturate. If it is the onset temperature of superconducting intergrain Josephson coupling, the FC susceptibility has a minimum at the transition temperature and may have a maximum at a temperature below the transition, as we learn from the magnetic data for  $\text{Ru}_{1-x}\text{Sr}_2\text{GdCu}_{2+x}\text{O}_{8-y}$  (Ref. [21]) and for  $\text{Bi}_2\text{Sr}_{2-x}\text{La}_x\text{CuO}_{6+y}$  (Ref. [22]). Moreover, it has been shown experimentally that the remanence disappears above the onset temperature of intergrain Josephson coupling [22].

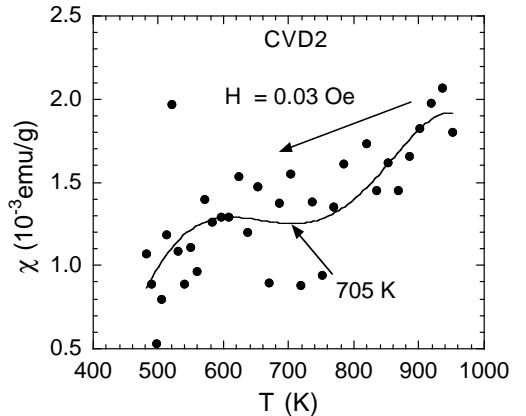


FIG. 4. The expanded view of the field-cooled susceptibility in 0.03 Oe below 950 K. The solid line is the forth-order polynomial fit. The fifth-order polynomial fit does not improve the fit quality, so we cut to the forth order.

Fig. 4 shows an expanded view of the field-cooled susceptibility in 0.03 Oe below 900 K. Because of the data scattering, we fit the data using a forth-order polynomial function. The fifth-order polynomial fit does not improve the fit quality, so we cut to the forth order. From the fitted curve, we see that there is a minimum at about 705 K and a maximum at about 600 K below which the susceptibility decreases with temperature significantly. The significant drop in the FC susceptibility below 600 K is inconsistent with a ferromagnetic/ferrimagnetic transition. Therefore, the combined data of Fig. 3b and Fig. 4 indicate that the transition at about 700 K is related to the onset temperature of superconducting intergrain Josephson coupling. Further, the field dependencies of the transition temperature have been extensively studied in other two samples (see below). The very strong field dependence of the transition temperature (see Fig. 7a and

Fig. 13a below) effectively rules out a magnetic origin of the transition at about 700 K.

### B. Superconductivity in sample CVD1

Fig. 5a shows the temperature dependencies of the FC susceptibility for sample CVD1 with different magnetic fields. One can see that there is a ferromagnetic/ferrimagnetic phase transition with the Curie temperature  $T_C = 855$  K. The transition temperature is independent of the magnetic field within the experimental uncertainty, as expected for a ferromagnetic/ferrimagnetic transition. From the  $T_C$  value, we can conclude that the sample contains  $\text{Fe}_3\text{O}_4$  magnetic impurities. From the measured magnetic hysteresis loop at 300 K, we obtain the saturation magnetization of 1.4 emu/g. Given the saturation magnetization of  $\text{Fe}_3\text{O}_4$  is 92 emu/g at room temperature, we estimate sample CVD1 has 1.5%  $\text{Fe}_3\text{O}_4$  magnetic impurities. If we compare the ferrimagnetic component of the susceptibility for sample CVD2 (Fig. 1d in 0.08 Oe) with that for sample CVD1 (Fig. 5a in  $-0.06$  Oe), we find that the former is smaller than the latter by a factor of about 5. These results indicate that the low field ferrimagnetic susceptibility is proportional to the magnetic impurity concentration. This should be the case when the average demagnetization factors for different types of magnetic impurities are the same.

Fig. 5a shows a remarkable feature: Above the Curie temperature the susceptibility is negative at low fields and becomes positive at higher fields. In Fig. 5b, we plot the susceptibility at 1000 K as a function of the magnetic field. In the low field region, there are large diamagnetic susceptibilities. For instance, the susceptibility in a field of  $-0.06$  Oe is  $-1.13 \times 10^{-3}$  emu/g, corresponding to about 3% of the full Meissner effect. Because the sample had experienced a negative field of about 200 Oe before it entered the sample space with a field of  $-0.06$  Oe, there would be a negative remanent magnetization at 1000 K if the sample contained hard magnetic impurities with Curie temperatures higher than 1000 K. The existence of the magnetic remanence *would* reduce the diamagnetic susceptibility for the negative applied field so that the diamagnetic contribution in Fig. 5b would be *underestimated*. However, since the susceptibility is reversible for the warm-up and cool-down measurements above 870 K, the remanence is negligible and thus there is no significant ferromagnetic/ferrimagnetic component in the data of Fig. 5b.

From the field dependence of the susceptibility at 1000 K, one can see that there are two components that compete with each other. One component is the diamagnetic susceptibility with the magnitude increasing with decreasing field. The second component is the paramagnetic susceptibility with the magnitude also increasing with decreasing field. In order to explain the field depen-

dence, one must assume that the magnitude of the diamagnetic susceptibility in the low field region increases

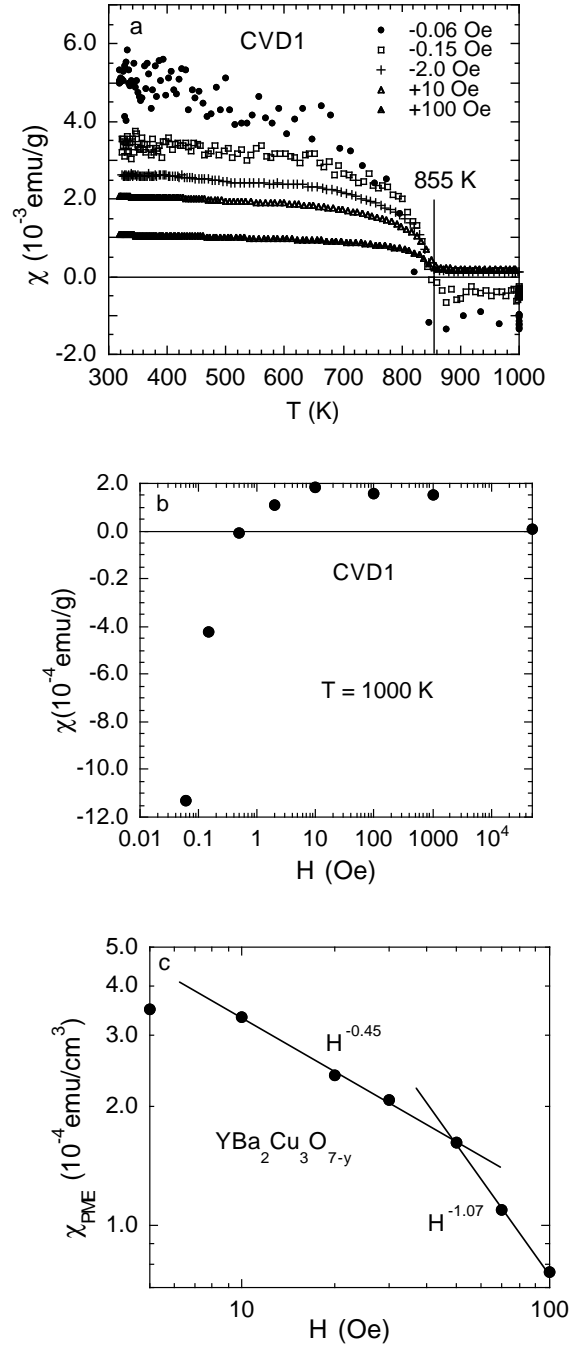


FIG. 5. a) The temperature dependence of the FC susceptibility for sample CVD1 with different magnetic fields. The ferrimagnetic component of the susceptibility at 600 K is about  $5.2 \times 10^{-3}$  emu/g in  $-0.06$  Oe and  $9.8 \times 10^{-4}$  emu/g in 100 Oe. b) The susceptibility at 1000 K as a function of the magnetic field for sample CVD1. c) The field dependence of the paramagnetic Meissner susceptibility for a twinned  $\text{YBa}_2\text{Cu}_3\text{O}_{7-y}$  crystal at  $0.96T_c$ . The data for  $\text{YBa}_2\text{Cu}_3\text{O}_{7-y}$  are extracted from Fig. 6 (sample 1) of Ref. [26].

much faster with decreasing field than the paramagnetic susceptibility while the reverse is true in the higher field region. Indeed, for a granular superconductor, the lower critical field tends to zero due to a very large intergrain penetration depth. So the magnitude of the diamagnetic susceptibility in the low field region increases faster than  $1/H$  (see Ref. [21–23]). On the other hand, the field dependence of the paramagnetic Meissner susceptibility for a known superconductor can be used for comparison. Fig. 5c shows the field dependence of the paramagnetic Meissner susceptibility at  $0.96T_c$  for a twinned  $\text{YBa}_2\text{Cu}_3\text{O}_{7-y}$  crystal. The data are extracted from Ref. [26]. We can clearly see that below 10 Oe, the field dependence of the PME is very weak. In the field range between 10 Oe and 50 Oe, the PME follows a power law  $H^{-\beta}$  with  $\beta = 0.45$ . Above 50 Oe, the PME depends more strongly on the field, leading to  $\beta = 1.07$ . Therefore, the result shown in Fig. 5b can be well explained in terms of the sum of the diamagnetic susceptibility due to diamagnetic screening currents and the paramagnetic susceptibility due to circulating currents around vortices (PME).

It is interesting to note that the magnetic contamination in CVD1 (1.5%) is much higher than that (0.3%) in sample CVD2 while the susceptibility at 1000 K for the former is smaller than that for the latter by about  $2.8 \times 10^{-3}$  emu/g in the field of 0.06 Oe. This implies that the magnitude of the paramagnetic susceptibility is anti-correlated with the magnetic impurity concentration. This rules out magnetic impurities as the origin of the paramagnetism. Alternatively, we can well explain this anti-correlation if the paramagnetic susceptibilities in these samples arise from the paramagnetic circulating currents around vortices. Much higher magnetic impurities in sample CVD1 may significantly suppress the surface superconductivity, which may in turn invalidate the condition  $H_{c3}(T) > H_{c2}(T)$  and thus suppress the PME according to the MQB model [19]. That is why the diamagnetic Meissner effect wins over the PME for the most impure sample in low fields.

In Fig. 3 and Fig. 4, we have shown that there is an onset of intergrain Josephson coupling for sample CVD2. The onset temperature is about 700 K in a magnetic field of 0.03 Oe. For sample CVD1, we should similarly expect to find intergrain Josephson coupling although

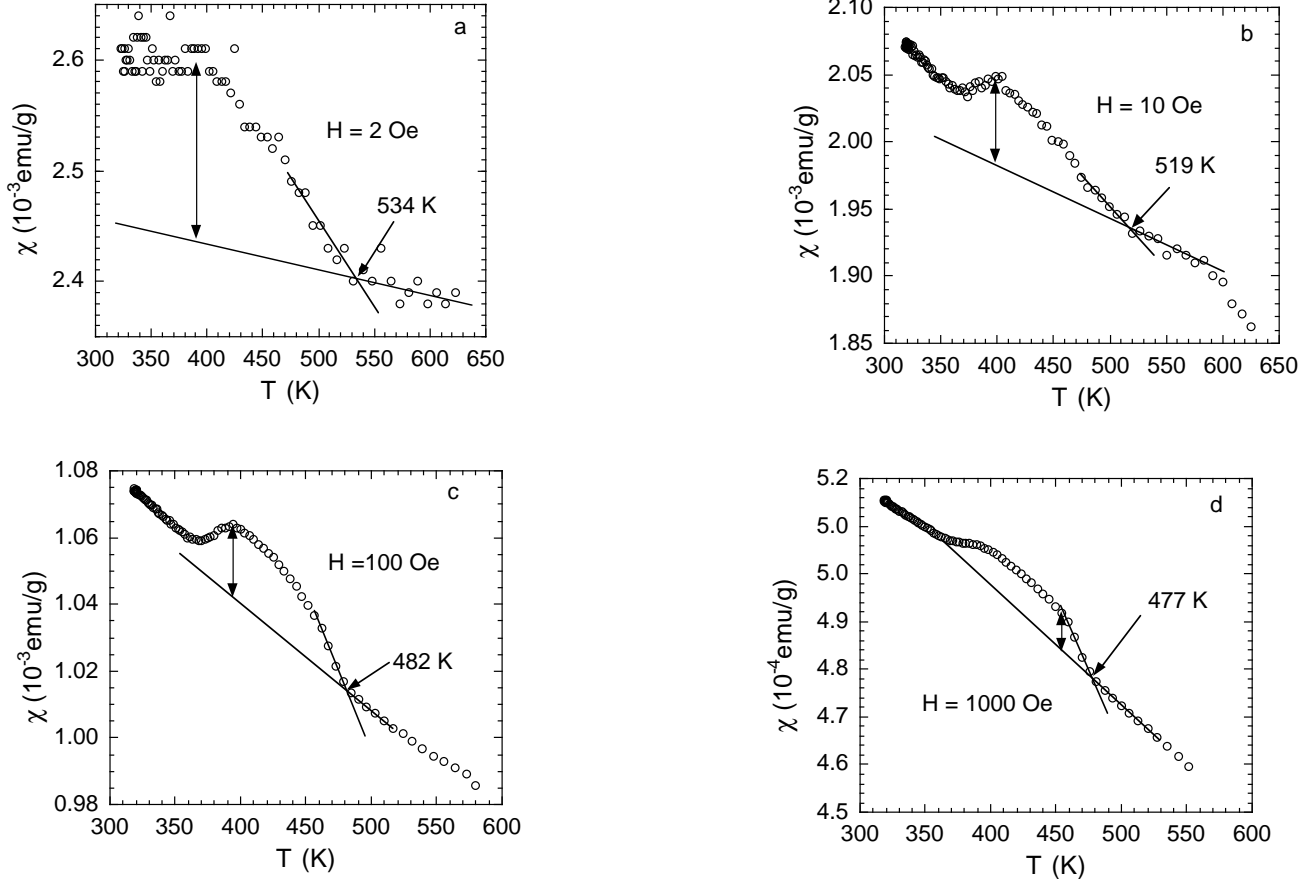


FIG. 6. The expanded views of the FC susceptibility for sample ARC in the magnetic fields of a) 2 Oe, b) 10 Oe, c) 100 Oe, and d) 1000 Oe.

the onset temperature may be different. In Fig. 6, we show expanded views of the FC susceptibility for sample CVD1 with different fields. In this temperature region, the susceptibility of the ferrimagnetic impurities increases weakly with decreasing temperature (a negative slope). There is additional onset of paramagnetism, which is clearly seen in all the figures. As we have seen [21] in  $\text{Ru}_{0.6}\text{Sr}_2\text{GdCu}_{2.4}\text{O}_{8-y}$ , the onset temperature  $T_{cJ}$  of intergrain coupling corresponds to the onset of the paramagnetism if the susceptibility has a dip-like feature, and to the onset of the diamagnetism if there is a shoulder-like feature. In the present case, there appears

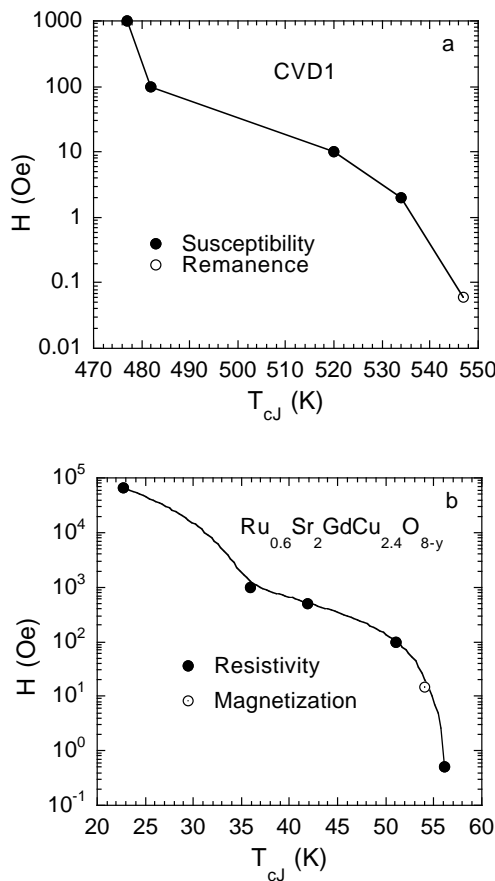


FIG. 7. The field dependence of the onset temperature  $T_{cJ}$  of intergrain Josephson coupling for a) sample CVD1 and b) a granular superconductor  $\text{Ru}_{0.6}\text{Sr}_2\text{GdCu}_{2.4}\text{O}_{8-y}$  (Ru-1212).  $T_{cJ}$  for Ru-1212 is defined as the onset of the paramagnetism in the FC magnetization data in Fig. 3 of Ref. [21] and as the midpoint of the resistive transition in Fig. 6 of Ref. [21]. The field dependence of  $T_{cJ}$  has a similar form for both systems, suggesting the same physical origin: Intergrain Josephson coupling. The strong field dependence of  $T_{cJ}$  rules out a magnetic origin of the transition.

to be dip-like features if one considers the fact that the background ferrimagnetic susceptibility has a negative slope in this temperature region. So it is reasonable to

assign the crossing temperature of the two straight lines to be  $T_{cJ}$ . It is interesting that in addition to the onset of paramagnetism at  $T_{cJ}$ , there is also an onset of the diamagnetism below  $T_{cJ}$ , similar to the case for sample CVD2 (see Fig. 4) and for some high-temperature superconductors (see Fig. 3b and Fig. 10 in Ref. [29]). From Fig. 6, we also estimate the paramagnetic Meissner susceptibility contribution, as indicated by the bi-directional arrows.

In Fig. 7a, we plot  $T_{cJ}$  as a function of the magnetic field. The  $T_{cJ}$  value deduced from the remanent magnetization (see below) is also included in this figure. One can see that  $T_{cJ}$  very strongly depends on the magnetic field, which is a hallmark of intergrain Josephson coupling. Further,  $T_{cJ}$  for sample CVD1 (Fig. 7a) is lower than that for sample CVD2 (Fig. 3b and Fig. 4) by about 180 K in the low field region. This may be due to the fact that more magnetic impurities in sample CVD1 suppress the Josephson coupling strength. In Fig. 7b, we show the field dependence of  $T_{cJ}$  for the granular superconductor  $\text{Ru}_{0.6}\text{Sr}_2\text{GdCu}_{2.4}\text{O}_{8-y}$ .  $T_{cJ}$  is defined as the onset of the paramagnetism in the FC magnetization data in Fig. 3 of Ref. [21] and as the midpoint of the resistive transition in Fig. 6 of Ref. [21]. Fig. 7b clearly indicates that two definitions are consistent. By comparing Fig. 7a with Fig. 7b, we can see that the field dependence of  $T_{cJ}$  has a similar form for both systems, suggesting the same physical origin: Intergrain Josephson coupling. The strong field dependence of  $T_{cJ}$  rules out a magnetic origin for the transition.

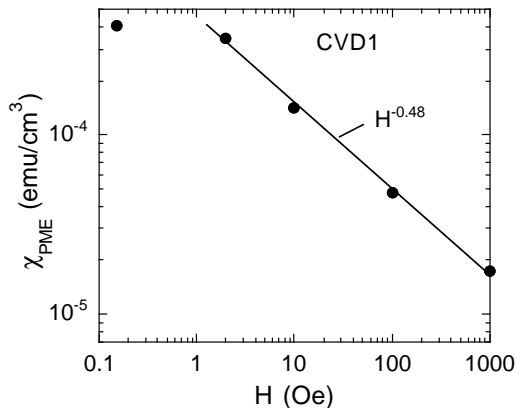


FIG. 8. The field dependence of the maximum paramagnetic Meissner susceptibility for sample CVD1 below the onset temperature of intergrain Josephson coupling.

In Fig. 8, we plot the maxima in the paramagnetic Meissner susceptibility as a function of the magnetic field for sample CVD1. The field dependence of the paramagnetic Meissner susceptibility is very weak below 2 Oe. Above 2 Oe, the field dependence follows a power law  $H^{-\beta}$  with  $\beta = 0.48$ . The  $\beta$  value for sample CVD1 is close to that (0.45) for a twinned  $\text{YBa}_2\text{Cu}_3\text{O}_{7-y}$  crystal

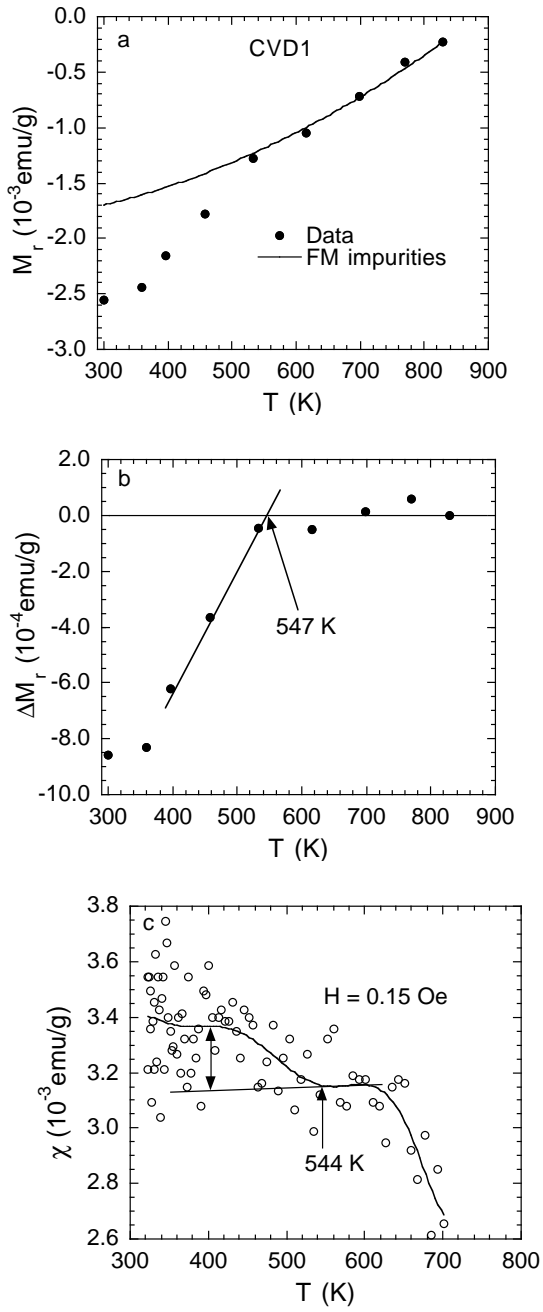


FIG. 9. a) The temperature dependence of the remanent magnetization for sample CVD1. The solid line is the ferrimagnetic (FM) contribution from impurities. b) The temperature dependence of the net remanent magnetization with the ferrimagnetic component subtracted from the data of Fig. 9a. This yields the superconducting component of the remanence with  $T_{cJ} = 547$  K. c) The expanded view of the field-cooled susceptibility for sample CVD1 in 0.15 Oe below 700 K. The data indicate  $T_{cJ} = 544$  K.

(see Fig. 5c). Moreover, the magnitudes of the PME for sample CVD1 and  $\text{YBa}_2\text{Cu}_3\text{O}_{7-y}$  are quite close in the field region where the PME follows a similar power law. This suggests that the PME for sample CVD1 below the

onset temperature of intergrain coupling is similar to the PME in the twinned  $\text{YBa}_2\text{Cu}_3\text{O}_{7-y}$  crystal.

In Fig. 9a, we show the remanent magnetization for sample CVD1. The small paramagnetic contribution has been subtracted. The data above 530 K can be well fitted by an equation  $M_r(T) = M_r(0)[1 - (T/T_C)^{2.07}]$  (see the solid line) with a fixed  $T_C = 855$  K. Comparing Fig. 9a with Fig. 3a, we can see that the ferrimagnetic remanent magnetization at 300 K for sample CVD1 is larger than that for sample CVD2 by a factor of 2.6. This is reasonable because sample CVD1 contains 1.5%  $\text{Fe}_3\text{O}_4$  impurities while sample CVD2 contains about 0.3%  $\gamma\text{-Fe}_2\text{O}_3$  impurities. Fig. 9b shows the net remanent magnetization for the second component. It is remarkable that the net remanent magnetization at 300 K for sample CVD1 (Fig. 9b) is almost the same as that for sample CVD2 (Fig. 3b) although the concentrations of the magnetic impurities in the two samples differ by a factor of about 5. This also suggests that this transition at  $T_{cJ}$  is not related to a ferromagnetic/ferrimagnetic transition, but consistent with what one expects if the source of this remanence is superconductivity of the nanotubes.

As seen from Fig. 9b, the second component has a transition temperature of about 547 K. This transition temperature should be similar to  $T_{cJ}$  obtained from the susceptibility data in a similar field. Fig. 9c shows an expanded view of the field-cooled susceptibility in 0.15 Oe below 700 K. Because of the data scattering, we fit the data using the 6th-order polynomial function. From the fitted curve, we see that there is a dip feature at about 544 K, very close to  $T_{cJ}$  deduced from remanent magnetization. This indicates that the superconducting remanent magnetization in sample CVD1 also disappears above  $T_{cJ}$ , similar to the case of sample CVD2. Nevertheless, we cannot rule out the existence of a small superconducting remanent magnetization above  $T_{cJ}$ , which could be masked by the large remanent magnetization contributed from magnetic impurities. The reversible magnetization for the warm-up and cool-down measurements in the temperature region of 860-1000 K suggests that any lingering remanent magnetization becomes negligibly small in this temperature region and that there is a negligible concentration of ferromagnetic impurities that have Curie temperatures higher than 860 K and coercivities higher than 0.06 Oe.

### C. Superconductivity in sample ARC

Fig. 10a shows the temperature dependence of the magnetization in a field of 0.03 Oe for sample ARC. For the warm-up magnetization, it is the sum of the remanent magnetization (after being exposed to the aforementioned negative 200 Oe motor field) and the intrinsic magnetization in 0.03 Oe. The negative remanent magnetization should disappear above the Curie temperature (870 K) of the  $\text{Fe}_3\text{O}_4$  impurities. From the measured

field-cooled susceptibility in 100 Oe from 1000 K to 300 K for another ARC sample with a mass of 14.6 mg, we find that the sample contains magnetic impurities with a Curie temperature of about 870 K. The magnetic impurities in sample ARC should also be  $\text{Fe}_3\text{O}_4$  because it has a similar Curie temperature. From the FC data, we estimate that the ferrimagnetic susceptibility of the  $\text{Fe}_3\text{O}_4$  impurities is about  $3.1 \times 10^{-6}$  emu/g at 600 K. By comparing the FC susceptibility in the same field (100 Oe) (see the caption of Fig. 5a) we find that the  $\text{Fe}_3\text{O}_4$  concentration in sample ARC is lower than that (1.5%) for sample CVD1 by a factor of 318. This indicates that sample ARC contains about 46 ppm  $\text{Fe}_3\text{O}_4$  impurities.

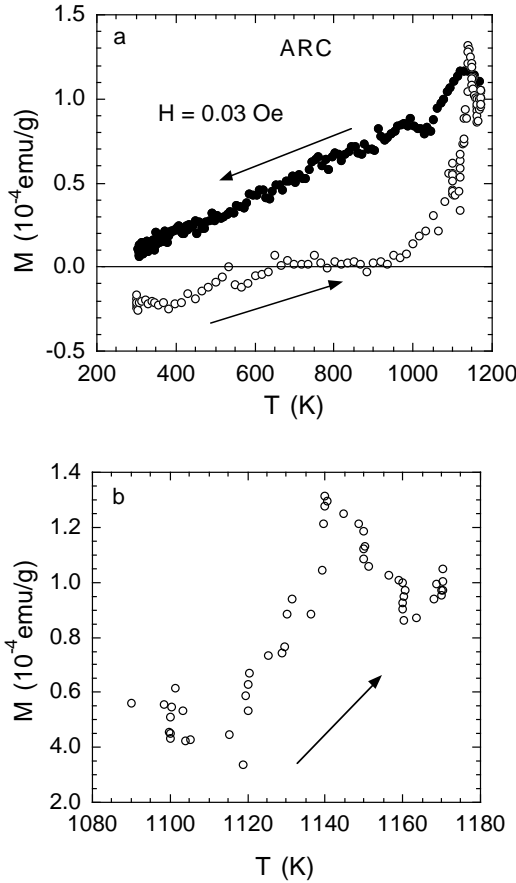


FIG. 10. a) The temperature dependence of the magnetization in a field of 0.03 Oe for sample ARC. b) The expanded view of the magnetization above 1090 K.

It is interesting to note that the negative magnetization disappears above 700 K and that there is a small temperature-independent positive magnetization between 700 K and 900 K. Above 900 K, the magnetization increases sharply, reaches a peak at about 1142 K and then drops sharply between 1142 K and 1170 K. When the sample is cooled down from 1170 K, the magnetization does not go back to the warm-up curve, showing a significant hysteresis. This is in contrast to the

reversible behavior of the magnetization between 1000 K and 1100 K for sample CVD2 (see Fig. 1b).

In order to understand this discrepancy, we show in Fig. 10b a zoomed view of the magnetization above 1090 K. We can see that at the temperatures of 1100 K, 1120 K, 1140 K, 1150 K, 1160 K, and 1170 K, the magnetization shows step-like features. Because these temperatures are the set points of the VSM's temperature control system, the temperatures are stable at these set points. The rapid change in the magnetization at each of these stable temperatures indicates the existence of many metastable states. It appears that the system tends to relax to the higher magnetization states below the peak

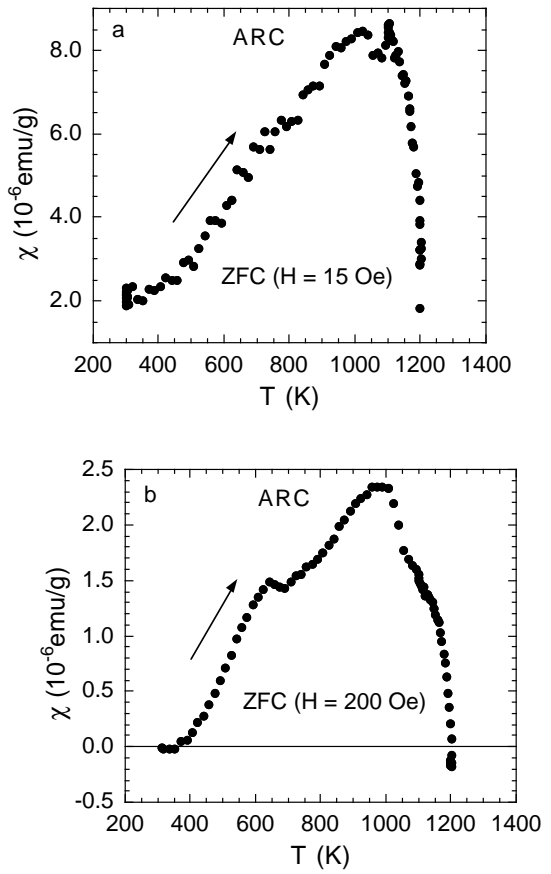


FIG. 11. The temperature dependences of the zero-field-cooled (ZFC) susceptibility for sample ARC in the magnetic fields of a) 15 Oe and b) 200 Oe.

temperature (1140 K) while it tends to relax to the lower magnetization states above the peak temperature. The jumps between the metastable states can be explained as magnetic flux quanta coming in or out [27]. The jumps between the metastable states should become more pronounced near the superconducting transition temperature because the Gibbs energies for the states with different orbital quantum numbers ( $L > 0$ ) are nearly degenerate [19]. The jumps between the metastable states

should become more pronounced near the superconducting transition temperature because the Gibbs energies for the states with different orbital quantum numbers ( $L > 0$ ) are nearly degenerate [19]. In the very low field range, only the diamagnetic  $L = 0$  state can exist just below the superconducting  $T_c$  while the paramagnetic  $L > 0$  states set in below a temperature  $T_1 < T_c$  (e.g.,  $T_1 = 0.98T_c$ ) [19]. Within this picture, only the diamagnetic Meissner effect exists in the temperature range between  $T_1$  and  $T_c$ . Below  $T_1$ , the metastable paramagnetic  $L > 0$  states set in and the paramagnetic Meissner effect can overwhelm the diamagnetic Meissner effect. Well below  $T_1$ , the differences of the Gibbs energies between the  $L > 0$  states and the  $L = 0$  ground state increase so that the system tends to go to the  $L = 0$  state. This can explain the peak feature just below  $T_1$  in the magnetization data, as observed in a Nb disk [20], MgB<sub>2</sub> polycrystalline sample [28], and sample ARC. For a field higher than  $H_{c3}(T)$  at temperatures above  $T_1$ , the system becomes normal above  $T_1$  and goes to the  $L = 0$  and the higher  $L$  states below  $T_1$ . If the  $L = 0$  state contributes a small diamagnetic Meissner effect in a higher field region, as

should be the case for granular superconductors, the paramagnetic Meissner effect will dominate in the whole temperature region below  $T_c$ . The above picture can explain the different hysteresis behaviors shown in Fig. 1b and Fig. 10a and the result shown in Fig. 16a below.

In Fig. 11a and Fig. 11b, we show the zero-field-cooled (ZFC) susceptibility in 15 Oe and 200 Oe, respectively. For the 15 Oe ZFC measurement, the sample was cooled from 1170 K to 300 K in “zero” field (0.03 Oe), and then the 15 Oe field was set at 300 K. For the 200 Oe ZFC measurement, the sample was cooled from 1200 K to 310 K in “zero” field (0.03 Oe), and then the 200 Oe field was set at 310 K. For the 15 Oe data, there is a shoulder feature near 700 K, corresponding to the onset of intergrain Josephson coupling [21]. A sharp peak is seen at 1105 K. Between 1105 and 1200 K, the susceptibility drops sharply with temperature, indicating the onset of the PME at about 1200 K. This implies that the superconducting transition temperature is slightly higher than 1200 K. For the 200 Oe data, there is a dip feature at about 690 K, corresponding to the onset of intergrain Josephson coupling [21]. A broad peak is seen at about 980 K. Between 1000 and 1200 K, the susceptibility drops

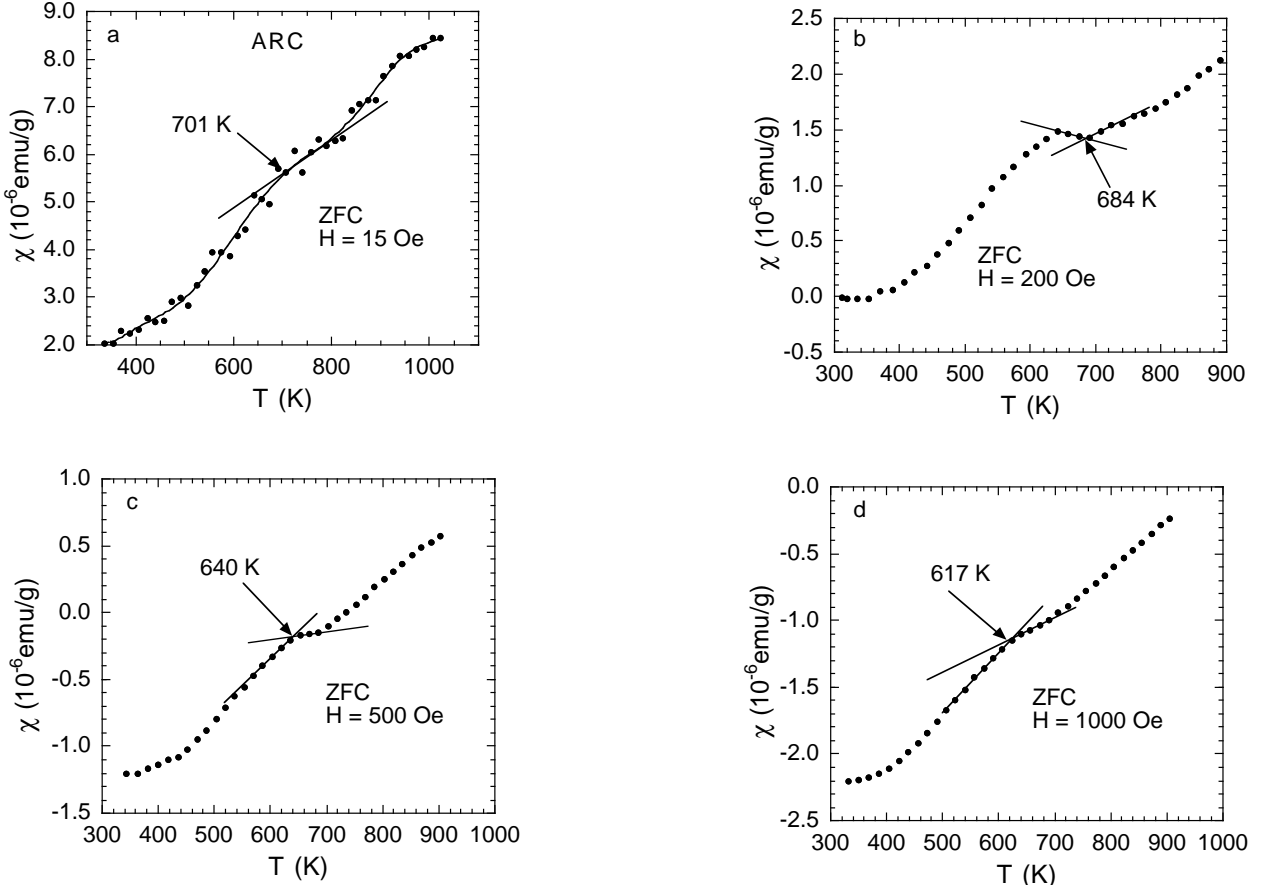


FIG. 12. The expanded views of the ZFC susceptibility for sample ARC in the magnetic fields of a) 15 Oe, b) 200 Oe, c) 500 Oe, and d) 1000 Oe.

sharply with temperature and even becomes negative at 1200 K. It is worth noting that all the measurements reported here are not real FC and ZFC ones because the samples have never been cooled in zero field above the superconducting transition temperature. Nevertheless, the samples are actually cooled in the (negative) earth field (about 0.5 Oe) above the transition temperature during the cooling process of sample preparation. This may produce a small negative remanent magnetization below  $T_{cJ}$  but has little effect on susceptibility data above  $T_{cJ}$ .

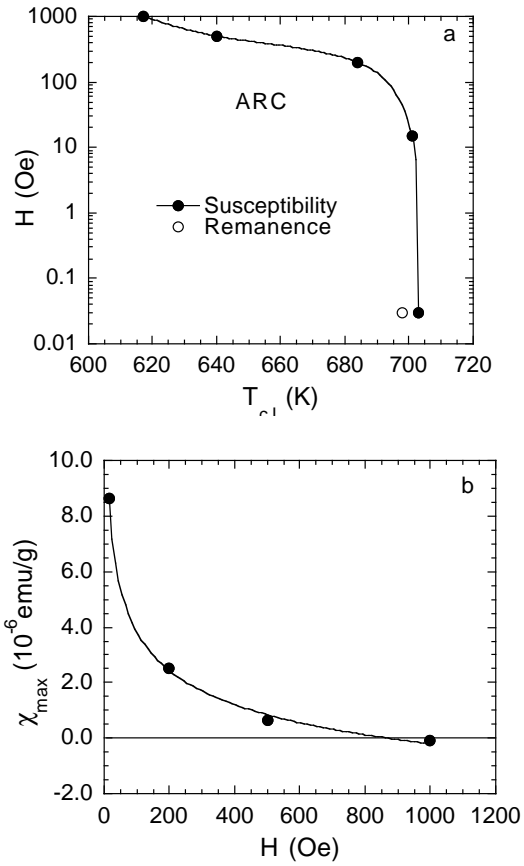


FIG. 13. The field dependencies of a) the onset temperature of intergrain coupling  $T_{cJ}$  and b) the peak ZFC susceptibility for sample ARC.

In Fig. 12, we show expanded views of the ZFC susceptibility in four different fields. For the 500 Oe and 1000 Oe ZFC measurements, the sample was cooled from 1200 K to 310 K in a field of about 2 Oe, and the fields were set at about 320 K. As we learn from the data [21] of  $\text{Ru}_{1-x}\text{Sr}_2\text{GdCu}_{2+x}\text{O}_{8-y}$ , the onset temperature  $T_{cJ}$  of intergrain coupling corresponds to the onset of the paramagnetism if there is a dip-like feature, and to the onset of the diamagnetism if there is a shoulder-like feature. For the 15 Oe, 500 Oe and 1000 Oe data, shoulder-like features are clearly seen, so  $T_{cJ}$  is defined as the onset of the diamagnetism. For the 200 Oe data, a dip-like feature is evident, so  $T_{cJ}$  is defined as the onset of the

paramagnetism.

Fig. 13a shows the field dependence of  $T_{cJ}$  for sample ARC. The  $T_{cJ}$  values determined from remanent magnetization (see Fig. 14a below) and from FC susceptibility (see Fig. 16b below) are also included in this figure. One can clearly see that the field dependencies of  $T_{cJ}$  for sample ARC (Fig. 13a), sample CVD1 and  $\text{Ru}_{0.6}\text{Sr}_2\text{GdCu}_{2.4}\text{O}_{8-y}$  (Fig. 7) are similar.

In Fig. 13b, we plot the peak ZFC susceptibility for four different fields. As the field increases, the peak susceptibility decreases and even crosses over to a negative value. Qualitatively, this field dependence is also consistent with the sum of a field-independent diamagnetic susceptibility and the paramagnetic susceptibility of ferrimagnetic impurities. This is because the field dependence of the paramagnetic Meissner magnetization [26] has a similar form as that of ferrimagnetic  $\text{Fe}_3\text{O}_4$ . The major difference in the field dependence of the magnetization between the two cases is that the applied field required for saturation is larger than 1000 Oe for the ferrimagnetic  $\text{Fe}_3\text{O}_4$  while it could be far less than 1 Oe for the paramagnetic Meissner effect. That is why the PME observed in a superconductor can be mistakenly explained in terms of possible contamination of ferrimagnetic impurities. Since the paramagnetic magnetization at 1100 K for sample ARC is close to that for sample CVD2 (compare Fig. 1b and Fig. 10a) while the magnetic impurities in the two samples differ by about two orders of magnitude, the observed large paramagnetic susceptibilities in these samples cannot arise from magnetic impurities. They are caused by the intrinsic PME in the multi-walled carbon nanotubes.

In Fig. 14a we show the remanent magnetization for sample ARC. These data are obtained from the warm-up magnetization data shown in Fig. 10a. The warm-up magnetization data can be decomposed into the remanent magnetization and non-remanent magnetization due to the nonzero field (0.03 Oe). The small constant magnetization between 700 K and 900 K in the warm-up data of Fig. 10a suggests that the negative remanent magnetization due to the  $\text{Fe}_3\text{O}_4$  impurities nearly cancels out the positive non-remanent magnetization in this temperature region. The remanent magnetization component is then obtained by using a few assumptions. One assumption is that the remanence at 300 K due to the 46 ppm  $\text{Fe}_3\text{O}_4$  impurities in sample ARC is smaller than that in sample CVD1 by a factor of 318, the ratio of the  $\text{Fe}_3\text{O}_4$  concentration between sample CVD1 and sample ARC. This is equivalent to assuming that the size of the impurities in sample CVD2 is the same as in sample ARC and that the temperature dependencies of the remanence in the two samples have the same functional form. Another assumption is that the remanence disappears above 870 K—the Curie temperature of  $\text{Fe}_3\text{O}_4$ . We also assume that  $T_{cJ} \simeq 700$  K so that the superconducting remanence disappears above 700 K.

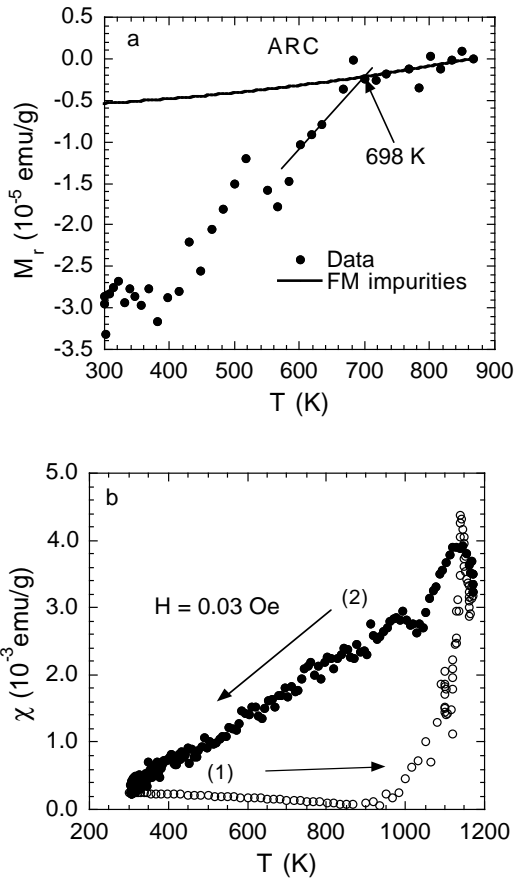


FIG. 14. a) The temperature dependence of the remanent magnetization for sample ARC. b) The temperature dependencies of the “intrinsic” warm-up and cool-down susceptibilities in 0.03 Oe obtained by subtracting the ferrimagnetic and superconducting remanences (Fig. 14a) from the raw experimental data (Fig. 10a). We remind the reader that since the measurements did not exceed  $T_c$ , the data are not strictly intrinsic.

By subtracting the superconducting and ferrimagnetic remanent magnetizations from the total warm-up magnetization (Fig. 10a), we can obtain the intrinsic warm-up susceptibility in 0.03 Oe, which is shown in Fig. 14b. It is interesting that the warm-up susceptibility has a negative slope below 900 K. A similar behavior was also seen in  $\text{YBa}_2\text{Cu}_3\text{O}_{7-y}$  crystals [26]. For comparison, we also include the cool-down susceptibility. It is remarkable that the paramagnetic susceptibility at the peak temperature is  $4.4 \times 10^{-3}$  emu/g. The magnitude of the PME is about 12% of the full Meissner effect. This percentage is in the range of 3-50% observed for high-temperature superconductors [29]. It is interesting to note that at 300 K, the cool-down susceptibility almost coincides with the warm-up susceptibility.

In order to further rule out magnetic contaminants as the origin of the observed large paramagnetic susceptibility above 1000 K, we show in Fig. 15 the magnetization as a function of the magnetic field at 320 K for sample

ARC. Above 20 kOe, the magnetization of any ferromagnetic impurity should be saturated and independent of the field. Between 20 kOe and 90 kOe, the data can be excellently fitted by a linear relation  $M = M_s + \chi_{dia}H$  with  $M_s = 9.27 \times 10^{-3}$  emu/g and  $\chi_{dia} = -8.66 \times 10^{-6}$  emu/g. The field independent diamagnetic susceptibility in the high-field region has also been observed in a granular superconductor  $\text{Ti}_2\text{Ba}_2\text{CuO}_{6+y}$  with  $T_c = 15$  K (see Fig. 7 of Ref. [23]). The deduced saturation magnetization from the fit would correspond to about 100 ppm magnetic impurities if the paramagnetic Meissner effect, which also contributes to the saturation magnetization [26], were not present. This implies that the upper limit of the total magnetic impurities is 100 ppm. Since sample ARC contains 46 ppm  $\text{Fe}_3\text{O}_4$  impurities, the upper limit of other magnetic impurities is about 54 ppm.

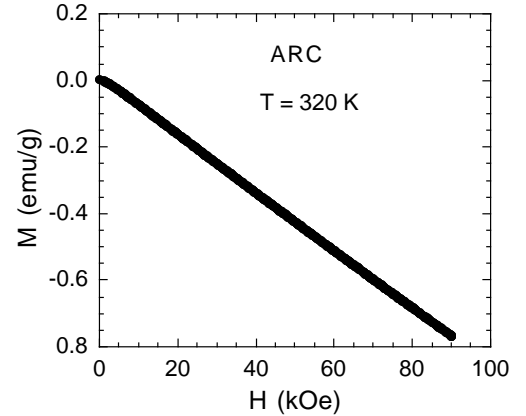


FIG. 15. The magnetization as a function of the magnetic field at 320 K for sample ARC. The data above 20 kOe can be excellently fitted by a linear relation  $M = M_s + \chi_{dia}H$  with  $M_s = 9.27 \times 10^{-3}$  emu/g and  $\chi_{dia} = -8.66 \times 10^{-6}$  emu/g.

Next, we argue that the concentration of the magnetic impurities in sample ARC is too small to account for the large paramagnetic susceptibility at 1140 K. We remind ourselves that for materials lightly contaminated with magnetic impurities having large permeabilities, the low field susceptibility is independent of the permeability and depends only on the shape and concentration of the contaminant. Shape effects are averaged out through a random orientation. Using this principle we begin with the assumption that the largest paramagnetic datum of sample ARC ( $4.4 \times 10^{-3}$  emu/g at 1140 K in Fig. 14b) is due to magnetic contaminants. By analogy to the results of sample CVD1—where 1.5% magnetic impurities corresponds to about  $5.2 \times 10^{-3}$  emu/g at 600 K (see the caption in Fig. 5a)—we find that were the data of Fig. 14b due to magnetic impurities there would be 1.3% magnetic contamination in sample ARC. However as discussion following Fig. 15 reveals, this far exceeds the upper limit of the contamination concentration. Thus we conclude that the concentration of the magnetic impurities in sample

ARC is too small to account for the large paramagnetic susceptibility and that the paramagnetic behavior is intrinsic and due to the PME.

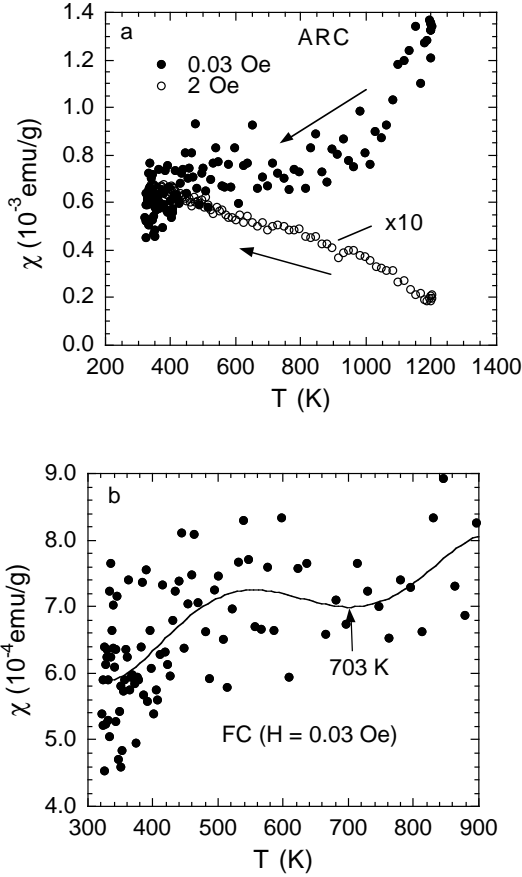


FIG. 16. a) The temperature dependence of the FC susceptibility of sample ARC in 0.03 Oe and 2 Oe. Before cooling in 0.03 Oe and 2 Oe, the fields were 15 Oe and 200 Oe, respectively. b) A zoomed view of the FC susceptibility in 0.03 Oe for sample ARC.

Fig. 16a shows the FC susceptibility of sample ARC in 0.03 Oe and 2 Oe. For the 0.03 Oe FC measurement, the field was set from 15 Oe to 0.03 Oe at 1200 K. For the 2 Oe FC measurement, the field was set from 200 Oe to 2 Oe at 1200 K. Similar to the case of  $\text{YBa}_2\text{Cu}_3\text{O}_{7-y}$  films [24], the susceptibility at 1200 K is inversely proportional to the field, or the magnetization at 1200 K is nearly independent of the field. Another remarkable feature shown in Fig. 16a is that the diamagnetic component in the field of 2 Oe is negligible compared with the paramagnetic component. This is similar to the results shown in Fig. 1d for sample CVD2 and Fig. 5a for sample CVD1. The strong field dependence of the diamagnetic component is associated with the granular nature of superconductivity. Comparing Fig. 14b with Fig. 16a, we also see that the magnitude of the susceptibility at 1170 K is much smaller in the case where the sample was cooled down from 1200 K. This discrepancy may be

related to the metastable nature of the states [19].

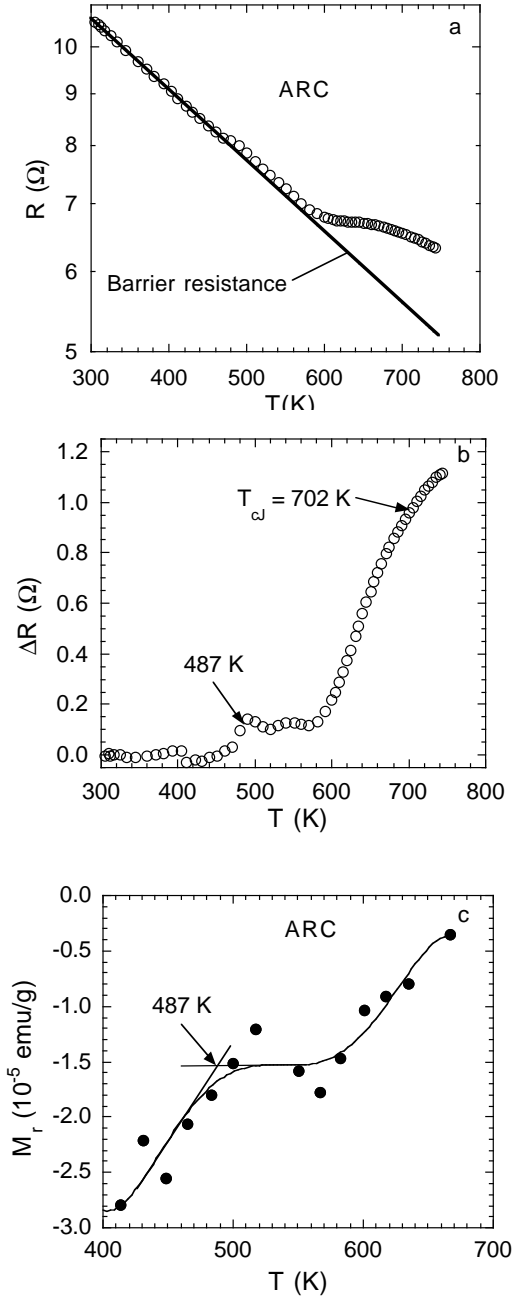


FIG. 17. a) The temperature dependence of the resistance for a mat of sample ARC. b) The resistance data that are subtracted by the fitted curve. c) The expanded view of the remanent magnetization for sample ARC. The resistance data are the same as those reported in Ref. [8] except the data are thinned for clarity. Two transitions at about 500 K and 700 K in the remanent magnetization data also emerge in the resistance data for the same sample.

In Fig. 16b, we show a zoomed view of the FC susceptibility in 0.03 Oe for sample ARC. Because of the significant data scattering, we fit the data with a forth order polynomial function. We can see the dip-like fea-

ture at about 703 K, which can be assigned as the onset temperature  $T_{cJ}$  of intergrain Josephson coupling.  $T_{cJ}$  deduced from these susceptibility data is also very close to that obtained from remanent magnetization (698 K, Fig. 14a).

We note that the susceptibility for sample ARC drops by  $1.4 \times 10^{-4}$  emu/g when the temperature is lowered from the peak temperature (about 560 K) to 340 K. On the other hand, the susceptibility for sample CVD2 drops by  $6.3 \times 10^{-4}$  emu/g when the temperature is lowered from the peak temperature (about 600 K) to 340 K. Therefore, the susceptibility drop for sample CVD2 is larger than for sample ARC by a factor of about 4.5. Similarly, the superconducting remanent magnetizations at 300 K for both sample CVD1 and sample CVD2 are larger than that for sample ARC by a factor of 36. This correlation is consistent with superconductivity.

In Fig. 17a we plot the previously published resistance data for a mat of sample ARC. The data are the same as those reported in Ref. [8] except the data are thinned here for clarity. It is interesting that the resistance decreases monotonically with increasing temperature below about 570 K. Above 570 K, the resistance tends to turn up. The resistance between 300 K and 450 K can be excellently described by  $17.3\exp(-T/618.3)$   $\Omega$ . This semiconducting-like resistance may come from the intertube barrier resistance for some weak Josephson links in the percolative network. In order to see more clearly the resistive transition, we plot in Fig. 17b the resistance data that are subtracted by the fitted curve. In addition to the major transition at about 700 K, consistent with the  $T_{cJ}$  value deduced from the magnetic data above, there appears to be a second transition at about 500 K. This second transition is also coincident with  $T_{cJ}$  from remanent magnetization data. In Fig. 17c, we show an expanded view of the remanent magnetization for sample ARC. The solid curve is fitted by a forth-order polynomial function. It is clear that the second transition at about 500 K in the resistance data is also seen in the remanent magnetization data. The one-to-one correspondence between the magnetic and electrical data in the same sample provides compelling evidence for hot superconductivity in multi-walled carbon nanotubes.

#### IV. CONCLUDING REMARKS

Our detailed magnetic studies on three different multi-walled carbon nanotube mat samples clearly indicate three distinct phase transitions. The first transition occurs at the temperature between 500 K and 720 K. The second transition is seen in the temperature between 855 K and 960 K, which is clearly identified as the ferrimagnetic transition of iron oxide contaminants. The third transition takes place at a temperature slightly higher than 1200 K. The first transition temperature depends very strongly on the magnetic field, and the field depen-

dence of the transition temperature is very similar to the field dependence of the onset temperature of intergrain Josephson coupling observed in granular superconductors. These results exclude *any* magnetic contaminants as the origin of this transition. Moreover, the transition temperatures determined from the remanent magnetization data, the susceptibility data, and the resistance data are all the same within the experimental uncertainty. These results unambiguously suggest that the first transition is related to the onset of intergrain Josephson coupling. Then it is natural that the third transition at about 1200 K is the intragrain superconducting transition.

The negligible superconducting remanent magnetization above the onset temperature of intergrain coupling is a natural consequence of granular superconductivity, as seen in high temperature superconductors [22,21]. The observed very large low-field paramagnetic susceptibility just below the third transition temperature  $T_c$  in the most pure sample and its strong field dependence exclude magnetic contaminants as the origin of the paramagnetism. These data can *only* be explained by the paramagnetic Meissner effect. The paramagnetic Meissner effect in the field of 0.03 Oe reaches about 12% of the full Meissner effect, which lies in the range (2%-50%) observed in high-temperature superconductors [29]. In addition to the large paramagnetic susceptibility near  $T_c$ , the susceptibility in 0.03 Oe decreases by  $4.1 \times 10^{-3}$  emu/g when the temperature goes from 1140 K to 300 K. This large drop in susceptibility (about 11% of the full Meissner effect in 0.03 Oe) is associated with the diamagnetic circulating currents (diamagnetic Meissner effect).

According to the MQB theory [19], the PME in small diameter superconducting wires is particularly strong because of the larger surface to volume ratio. This model can naturally explain why the Pb nanowire array with an average diameter of 40 nm is paramagnetic down to 2 K while the Pb nanowire array with a diameter of 60 nm is diamagnetic below  $T_c$  (Ref. [27]). There is also a second transition in the Pb nanowire array, which occurs at a temperature of about  $0.5T_c$  in the field of 50 Oe. The second transition temperature also strongly depends on the magnetic field, suggesting that the transition is also associated with the onset of interwire Josephson coupling. Interestingly, in our sample ARC, the onset temperature of the intergrain Josephson coupling is about  $0.58T_c$  if we take  $T_c = 1200$  K. Moreover, within the MQB model, the suppression of surface superconductivity by magnetic impurities tends to reduce the PME, so diamagnetic Meissner effect can win over the PME. That is why the most impure sample has a substantial diamagnetic susceptibility at 1000 K while the most pure sample has a large paramagnetic susceptibility at the same temperature.

In most cases, the PME is seen only in FC data [29]. In some cases, the PME is also seen in ZFC data of granular superconductors [22,28]. The authors of the MQB theory have assumed that the system only goes to the diamag-

netic  $L = 0$  state in the ZFC condition so that the PME does not exist in ZFC data. We do not think that this assumption is justified. Since all the  $L \geq 0$  states are the solutions of the Ginzburg-Landau equations in mesoscopic samples [19], they should be thermodynamic states that only depend on the field and temperature. For the  $L = 0$  state, the FC and ZFC diamagnetic susceptibilities are the same for superconducting samples without open holes. In the same way, for the  $L > 0$  states, the FC and ZFC paramagnetic susceptibilities should also be the same. Because Gibbs energies for all the states are quite close near  $T_c$ , the thermal energy should be large enough to make many high- $L$  states be occupied, leading to the paramagnetic Meissner effect. Because of the metastable nature of these states, the paramagnetic Meissner effect will strongly depend on the cooling or heating rate and on the field history if the sample never goes to the normal state.

For granular superconductors, the ZFC diamagnetic susceptibility in the  $L = 0$  state should be significantly larger than the FC susceptibility because the intergrain spaces behave like open holes for a field higher than the intergrain  $H_{c1}$ . Thus, the diamagnetic component in ZFC data is significantly larger than that in FC data, in agreement with experiment [22]. Further,  $H_{c1}$  tends to zero so that the diamagnetic susceptibility decreases rapidly with the field even in the low field region. This can explain why the diamagnetic component is not visible even for a field higher than 0.5 Oe in sample CVD1.

In future, we will push the measurement temperature up to 1273 K to see the complete superconducting transition. This will allow us to do real FC and ZFC measurements to obtain more meaningful data. Nevertheless, the present data are convincing enough to draw the conclusion that the multi-walled carbon nanotubes are very hot superconductors with a  $T_c$  slightly higher than 1200 K.

**Acknowledgment:** We thank Quantum Design (J. O'Brien, N. R. Dilley, J. J. Cherry, R. Fox, S. Gomez, and D. Polancic) for hospitality, use of the VSMs and technical assistance.

Correspondence should be addressed to  
gzhao2@calstatela.edu.

(1989).

- [5] S. M. Cui and C. H. Tsai, Phys. Rev. B **44**, 12500 (1991).
- [6] R. Saito, M. Fujita, G. Dresselhaus, and M. S. Dresselhaus, Appl. Phys. Lett. **60**, 2204 (1992).
- [7] H. Ajiki and T. Ando, J. Phys. Soc. Jpn. **62**, 1255 (1992).
- [8] G. M. Zhao and Y. S. Wang, cond-mat/0111268.
- [9] L. Merchant, J. Ostrick, R. P. Barber, Jr., and R. C. Dynes, Phys. Rev. B **63**, 134508 (2001).
- [10] G. M. Zhao, cond-mat/0208197.
- [11] G. M. Zhao, cond-mat/0208198.
- [12] G. M. Zhao, cond-mat/0208200.
- [13] G. M. Zhao, cond-mat/0208201.
- [14] G. M. Zhao, cond-mat/0307770.
- [15] G. M. Zhao, *Molecular Nanowires and Other Quantum Objects* edited by A. S. Alexandrov, J. Demsar and I. K. Yanson (Nato Science Series, Kluwer Academic Publishers, Netherlands, 2004) page 95-106.
- [16] G. M. Zhao, cond-mat/0412382.
- [17] G. M. Zhao, *Carbon nanotubes: New Research* edited by Frank Columbus (Nova Publisher, New York) in press.
- [18] Y. Kopelevich, R. R. da Silva, J. H. S. Torres, S. Moehlecke, and M. B. Maple, preprint.
- [19] V. V. Moshchalkov, X. G. Qiu, and V. Bruyndoncx, Phys. Rev. B **55**, 11793 (1997).
- [20] L. Pust, L. E. Wenger, and M. R. Koblischka, cond-mat/9807109.
- [21] P. W. Klamut, B. Dabrowski, S. Kolesnik, M. Maxwell, and J. Mais, Phys. Rev. B **63**, 224512 (2001).
- [22] H. H. Wen, W. L. Yang, Z. X. Zhao, and Y. M. Ni, Phys. Rev. Lett. **82**, 410 (1999).
- [23] C. Bergemann, A. W. Tyler, A. P. Mackenzie, J. R. Cooper, S. R. Julian, and D. E. Farrell, Phys. Rev. B **57**, 14387 (1998).
- [24] D. A. Luzhbin, A. V. Pan, V. A. Komashko1, V. S. Flis, V. M. Pan, S. X. Dou, and P. Esquinazi, Phys. Rev. B **69**, 024506 (2004).
- [25] J. P. Lu, Phys. Rev. Lett. **74**, 1153 (1995).
- [26] S. Riedling *et al.*, Phys. Rev. B **49**, 13283 (1994).
- [27] Shijun Yuan, Liyuan Ren, and Fashen Li, Phys. Rev. B **69**, 092509 (2004).
- [28] J. Horvat, X. L. Wang, S. Soltanian and S. X. Dou, cond-mat/0201006.
- [29] W. Braunisch *et al.*, Phys. Rev. B **48**, 4030 (1993).

---

- [1] A. S. Alexandrov and N. F. Mott, *Polarons and Bipolarons* (World Scientific, Singapore, 1995).
- [2] V.L. Ginzburg, in: V.L. Ginzburg, D. A. Kirzhnits Eds., *High-Temperature Superconductivity*, Consultants Bureau, New York, 1982.
- [3] W. A. Little, Phys. Rev. **164**, A1416 (1964).
- [4] Y. C. Lee and B. S. Mendoza, Phys. Rev. B **39**, 4776